# Identification and Update of Thermal Models in Digital Twins of ePowertrain Motors

Jon García Urbieta; Iñigo García; Marta Marijuán; Dr. Sergio Armentia
GKN Automotive, Zumaia, Spain

Dr. Pablo Díaz; Dr. Antonio J. Rodríguez, Dr. Francisco González
Laboratorio de Ingeniería Mecánica, Campus Industrial Ferrol - CITENI, Universidade da Coruña, Ferrol, Spain

Contact: jon.garcia@gknautomotive.com

**Abstract**

**Thermal phenomena are of critical importance in automotive applications of permanent-magnet synchronous motors (PMSMs). Heat accumulation in sensitive locations, such as the magnets or the endwindings, can decrease the performance of the device and damage it in extreme cases. Preventive actions can be defined based on the accurate knowledge of the temperatures of the device, but monitoring thermal effects through direct measurements is often unfeasible in production units. An alternative consists in building real-time capable digital twins to represent the thermal effects in the motor, using to this end a limited set of sensor data. Here, an approach to build these digital twins that relies on a Lumped-Parameter Thermal Network (LPTN) representation of the heat flows and temperatures in the PMSM is presented, whose predictions are fused with sensor information by means of state, input, and parameter observers. For the LPTN to provide a meaningful description of the motor behaviour, it is necessary to identify the relevant thermal effects that take place inside the device and translate them into appropriate parameters and input functions. Also, a methodology to adjust the LPTN from experimental readings obtained in a test bench by means of a combination of observer algorithms and sensitivity analysis is introduced. The method can be applied in the offline and online tuning of thermal models, enabling the update of real-time capable digital twins over extended periods of time and taking into consideration the long-term evolution of the system parameters caused, for instance, by thermal cycling deterioration and component aging. Results obtained in a cyber-physical bench, in which the motor under test was interfaced to a computer simulation of a vehicle motion, confirmed the ability of the methodology to improve the thermal representation of physical PMSMs.**

**Content**



## 1 Introduction

Novel automotive components and technologies require extensive testing campaigns before they can be released to the market, to meet the stringent safety standards and regulations of road transportation. Comprehensive testing campaigns are necessary to guarantee that new products and techniques will perform as intended during the design stage and to identify unexpected phenomena whose effect on performance is initially unknown. This way, testing becomes a key step to ensure the safe deployment of new solutions in real-world applications, and to generate the necessary confidence to have them accepted by the market and the consumers [1].

Road vehicles are nowadays complex engineering systems in which the interplay of mechanical, electronic, hydraulic, and thermal effects has an impact that needs to be considered not only at the design stage of new models, but also during the entire life cycle of the product, e.g., to enable predictive maintenance. In this context, traditional

testing approaches, based on the availability of a prototype of the final vehicle, need to be supported by alternative validation methods to reduce costs and accelerate development. Model-Based System Testing (MBST) is a recently proposed paradigm for the evaluation of automotive components [2], based on the combination of physical tests with simulation models to study the performance of multi-physics systems. Following a MBST approach, it is possible to assess the behavior of automotive components by testing them in System-in-the-Loop (SiTL) platforms, replacing the real-world environment with which the device under test (DUT) would interact in practice by its virtual representation and an appropriate combination of sensors and actuators. This assessment can take place before a full-vehicle prototype exists, thus allowing the early-stage testing of components in automotive systems under realistic conditions. The resulting cyber-physical test bench (CPTB) represents an application of MBST of particular interest for the automotive industry [3].

The practical use of CPTBs in industrial setups enables the realistic testing of components at a reduced cost, but requires addressing important challenges to ensure that the obtained results are reliable and representative of actual operation conditions.

CPTBs are hybrid co-simulation environments [4,5] that need to combine real-time execution with the monitoring of the accuracy of the overall dynamics [6, 7]. It is also necessary to verify and handle the effect of communication issues at the physical-virtual interface [8, 9], and to adapt the actuation strategies to the available information about the system operation point and the physical limitations of the hardware used in the bench. The treatment and use of the data gathered by the sensors mounted on the DUT and the bench itself is a point of particular interest. For instance, the use of appropriate estimation and data fusion algorithms enables one to gain insight into the operation of the system under study that goes beyond sensor readings, e.g., [10, 11], and can be used as a means to improve the knowledge gained from experimentation via the introduction of digital twins in the testing process [12]. With proper calibration and data treatments, costly tests could be performed in benches through the interaction with virtual environments, thus significantly reducing development costs.

This kind of test bench allows to start experimentation in the early stages of product development and enables a controlled enviroment for complex testing. By means of a virtual environment with a dynamic vehicle model, complemented with a digital twin of the eMotor, an easy change of simulation scenarios can be realized. Besides, a simpler instrumentation can be used in comparison to real vehicle applications; indeed, the use of benches makes it possible to acquire in a simple way sensor data such as the permanent magnet temperatures, which are complex to obtain in real vehicle tests. Besides, dangerous situations or emergency manoeuvres can be replicated without the need of destructive testing, and repeatability of situations and measurements' variability can easily be analyzed. Hence, in a large number of applications this can be translated in cost reduction, regarding prototype manufacturing, assemblying and testing, in man-hour for test setting and troubleshooting and even in eliminating some of the eMotor physical sensors thanks to digital twins.

Figure 1 provides a schematic of the benefits of introducing MBST methodologies, such as CPTBs, in product development cycle. If a traditional, prototype-based approach is followed, most design defects cannot be identified until a full-system prototype is available for experimentation. However, it is precisely during the early stages of the cycle when design modifications can be performed most easily, as the costs of removing a defect increase as design decisions and implementations accumulate over time. MBST schemes, conversely, allow to identify some of these problems as soon as components are available for experimentations, provided that appropriate testing facilities can be used to this end.

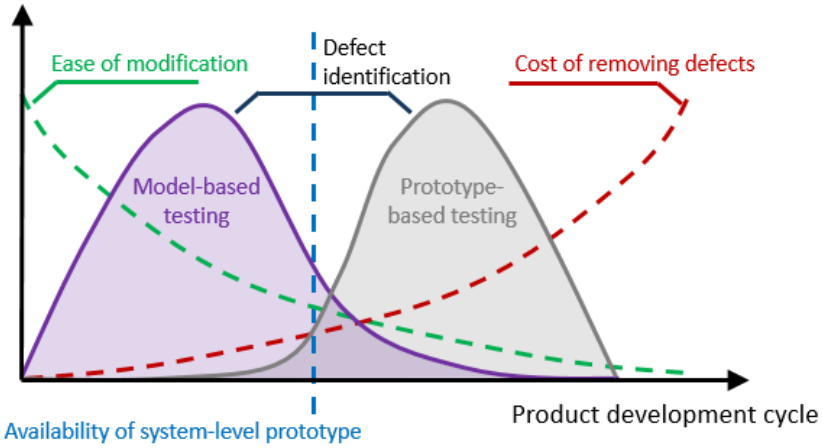


Fig. 1 Impact of Model-Based System Testing methodologies on product development cycle.

The CPTB used for the generation of the data in this article has been designed to evaluate the mechanical, electric, and thermal behavior of permanent-magnet synchronous motors (PMSMs), the most frequently used type of electric drive in automotive ePowertrains, by virtue of their compactness, high power density, and higher performance efficiency compared to other eMotor types. In particular, thermal effects play a major role in the operation and behavior of PMSMs [13, 14]. During operation, heat is generated at locations such as the eMotor windings and magnets, increasing component temperatures and making it necessary to employ cooling methods [15], because excessive temperature can cause permanent damage to the motor magnets [16]. At the same time, however, the optimal operation of electric drives requires them to perform as close as possible to their admissible temperature thresholds. The control algorithms that regulate this operation need to rely on precise information about the eMotor temperatures to attain this goal [17]. This is problematic, because temperature sensors can be placed at some locations on the component, but often not at the most critical ones, e.g., the magnets, especially in practical applications.

Efficient computational models of the thermal effects in PMSMs can be used to address this issue and provide an indication of the internal temperatures of the eMotor. Lumped-parameter thermal networks (LPTNs) offer a good trade-off between accuracy and real-time execution capabilities. It is necessary, however, to adjust their topology, inputs, and parameters to match the behaviour of the physical system that they represent, which is not always straightforward. Theoretical approaches to determine model

parameters are not completely accurate; moreover, these values in physical components are subjected to uncertainty [18]. Besides, the thermal parameters of an LPTN may vary during operation, as a result of changing operation conditions or the aging of materials [19], for instance. State, input, and parameter estimation algorithms have been proposed as a way to overcome the above-mentioned problems. LPTNs, in particular, lend themselves well to sensor data fusion by means of Kalman filters, which enables the definition of estimators based on temperature readings from sensors mounted on the DUT [12], [20], [21]. With appropriate statistical treatments of the gathered data, these solutions can become the basis to develop digital twins to accurately describe the thermal behavior of the components tested in CPTBs.

In this kind of bench, the assessment of the thermal behavior of the tested device is based upon an adjustable computational representation of the thermal dynamics of the system. Readings from thermocouples mounted on accessible locations on the DUT are fused with a detailed LPTN that models the thermal behavior of the component, to develop a state, input, and parameter estimation algorithm, able to adjust the system model based on sensor readings. This approach had been previously used in [12] in the offline estimation of thermal properties of electronic components.

In this study, a methodology for the construction of such digital replicas is introduced. A LPTN representation of the motor is employed to model the intricate interplay of heat fluxes and temperature distributions within the PMSM. The anticipatory outcomes of this model are then merged with data from sensors through the implementation of observers that account for the system state, input, and parameters. The approach can be employed for both offline and online refinement of thermal models, facilitating the ongoing enhancement of real-time adaptable digital counterparts for extended durations. This encompasses the integration of alterations arising from the extended temporal evolution of system parameters, prompted by factors such as thermal cycling degradation and component maturation. Outcomes derived from experimentation conducted on a cyber-physical platform, where the examined motor was interconnected with a computer-simulated vehicle motion, corroborated the effectiveness of this methodology in enhancing the fidelity of thermal portrayals for tangible PMSMs.

Firstly, in Section 2, a detailed description of the CPTB and its capabilities is presented. In Section 3 a calibration procotol is described, based on dynamic sensitivity analysis and optimization of the most influential parameters. The method is applied to the improvement of an LPTN model in a WLTP cycle. In the investigation shown in Section 4, the use of the CPTB was extended to the online correction in an experimental setup of the inputs of LPTNs that represent PMSMs, to support the notion that it can be used in real-time operations with physical components in test benches. Experimental runs of the test bench were used to correct uncertain input values, both offline and during runtime; results confirmed that the thermal estimation algorithm was able to automatically adjust the LPTN representation to deliver realistic predictions of the thermal dynamics of the motors under test. In Section 5, an experimental campaign is conducted to determine the law of deterioration of an automotive-grade stator insulation system. The result will also be used to update models depending on the ageing state of the motors. Finally, conclusions to the current investigation and future work are presented.

## 2 Cyber Physical Test Bench Design

The test bench used in this research has been designed to enable the evaluation of permanent-magnet, three-phase eMotors with a power of up to 150 kW, 450 $A_{rms}$ at each phase, maximum angular speeds of 16,000 rpm, and able to deliver an output torque of 220 Nm.

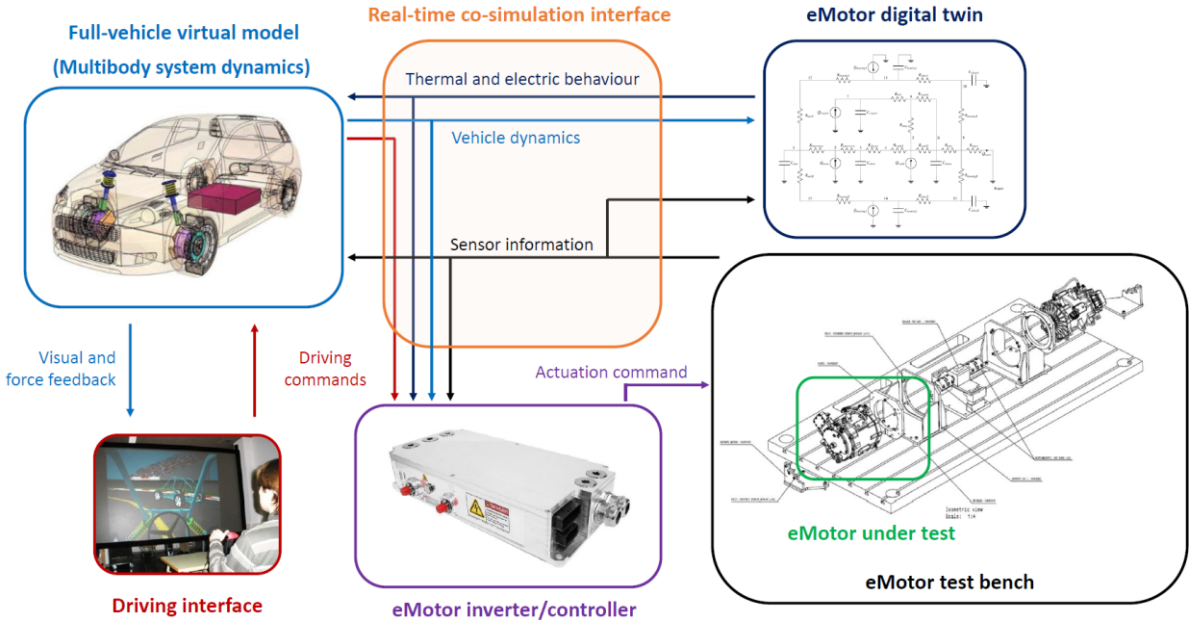


Fig. 2 Conceptual design and flow of information in a cyber-physical test bench for automotive-grade eMotors.

The bench intends to enable the evaluation of the tested motors in a controlled and repeatable environment, which is beneficial for the systematic gathering of experimental data and makes it easier and safer to reproduce dangerous situations such as emergency manoeuvres. This approach would not be simple, or even feasible to execute, if a prototype-driven strategy were to be followed.

For the particular case of electric motors, the evaluation of their thermal response is of interest for the design and improvement of efficient control algorithms that make the most of the component capabilities without compromising their safe operation, avoiding excessive temperatures that could damage them.

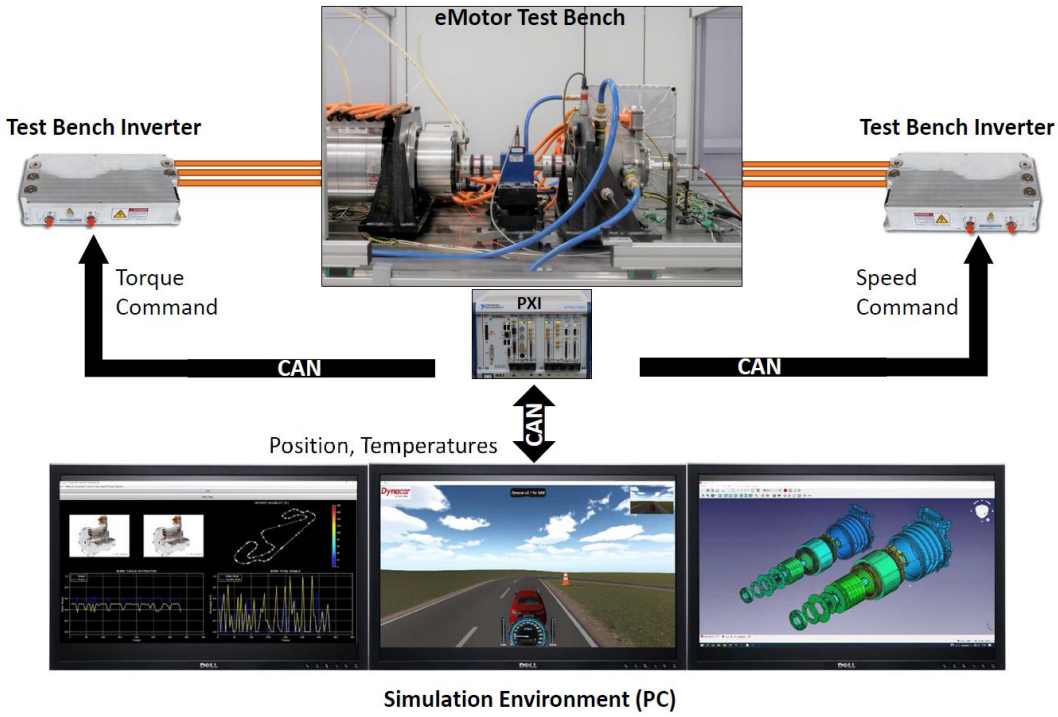


Fig. 3 Implementation and information flow in the proposed CPTB.

The bench is arranged in a back-to-back configuration [22]. The eMotor under study, i.e., the DUT, is actuated with a desired torque, determined by a human or virtual driver. The DUT is mechanically coupled to an identical component that drags it at the speed determined by a computer simulation of the virtual environment with which the DUT interacts. Each motor has its speed or torque commanded by means of a commercial inverter. A real-time co-simulation interface is responsible for the exchange of information between the components of the bench. Figure 2 illustrates the conceptual design of the test bench for ePowertrain motors used in this study.

Figure 3 illustrates the practical realization of the cyber-physical test bench. The communication between the physical ePowertrain components and the simulation environment is performed via CAN by means of a PXI bus, both for command delivery and test bench data acquisition.

A torque sensor is installed at the connection between the motor shafts; current probes provide readings of the electric state of the motor phases. These readings are used to determine the mechanical, electric, and thermal operation point of the eMotors. Besides, accelerometers are mounted on the bench platform to monitor system performance and to enable noise, vibration, and harshness (NVH) analyses.

Figure 4 provides a simplified illustration of the communications layout of the bench, in which the aforementioned sensors are connected to the central PC by means of a data acquisition system. These measurements are received by the CPTB, and can thus be compared in real time with the predictions delivered by the thermal model of the motor.

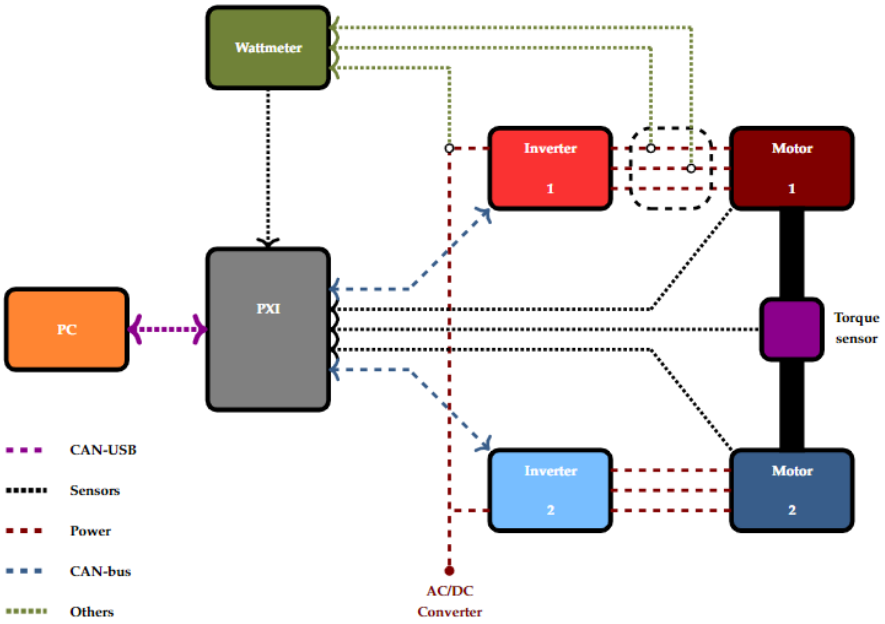


Fig. 4 Test bench communications layout.

Two levels of sensorization are considered for the DUTs. *Production* units present a basic set of NTC (Negative Temperature Coefficient) sensors, usually one or two in the winding of the stator, which often is not the hot spot of the eMotor. Hence, a correlation with the hot-spot temperature or a safety factor is usually needed for the definition of derating strategies, whose target is to maintain the eMotor in the temperature range desired to avoid shortening the lifespan of the machine. In the test bench, however, *Testing* units are provided with a higher number of sensors, placed near critical components. Hence, thermocouples are located in the gaps between the layers of conductors in the winding to measure the temperature as close to the conductors as possible, commonly in the endwindings and the extremes of the stator iron. Figure 5 shows an example of the distribution of the sensors installed in the eMotors under study.

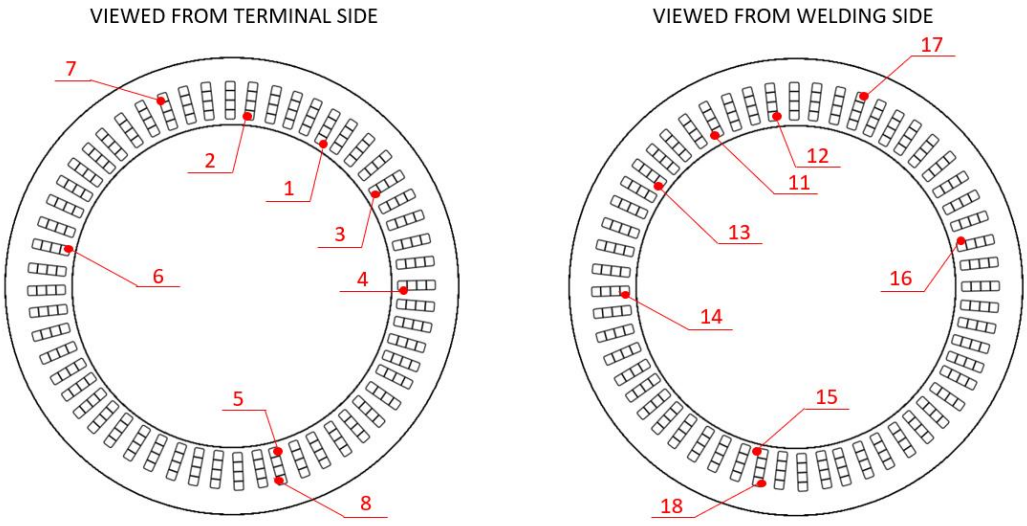


Fig. 5 Thermocouple locations in the stator of the eMotor.

Analogously, thermocouples are located in the rotor between chosen pairs of rotor stacks, both in the iron core and the magnets. Figure 6 presents an example of the instrumentation of the rotor to measure its most relevant temperatures. It is worth mentioning that it has been observed that temperatures in the same section locations vary along the axial longitude of the rotor, both in the magnets and the rotor core. Hence, two sets of sensors are placed in the shown example to capture this effect. The equipment used for the data retrieval is a wireless system. The first part is an emitter that is inserted in the shaft cavity, rotates solidary to the shaft and contains the thermocouples that are connected to the measurement points. The second part is a static receiver that is separated by a narrow airgap from the emitter. Thus, the emitter wirelessly transmits the read measurements to the receiver and subsequently the data is captured by a datalogger.

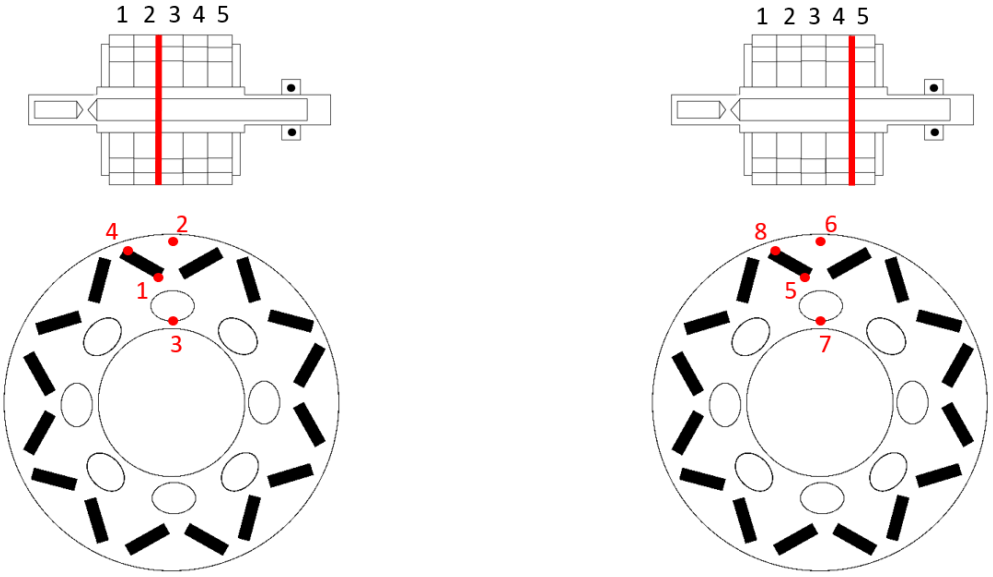


Fig. 6 Location of the thermocouples on the rotor.

## 2.1 Software components of the test bench

The simulation environment of the bench is built in Matlab-Simulink, following a modular block scheme. Figure 7 depicts its structure. It is composed of two main domains: the Vehicle and the eMotor.

The first domain (Vehicle) contains a multibody dynamics solver to simulate the vehicle motion with a visual interface for human drivers (Figure 3, center screen). Additional dedicated blocks evaluate the dynamics of the brakes, the battery, and the efficiency of the transmission.

The second domain (eMotor) describes the behaviour of the DUT; it is the starting point of a digital twin for the electromagnetic and thermal representation of the motor. Currently, this unit is composed by a loss block that determines the thermal losses of the eMotor, and its LPTN-based thermal representation. The losses module determines the copper losses produced in active and endwindings, both DC and AC, which are combined and applied to the corresponding node. Iron losses are calculated

per region, yoke and teeth for the stator and core and external diameter for the rotor. Magnet and mechanical losses are introduced here as well. Finally, a distribution block assigns the correct losses to the desired components as inputs in the thermal model.

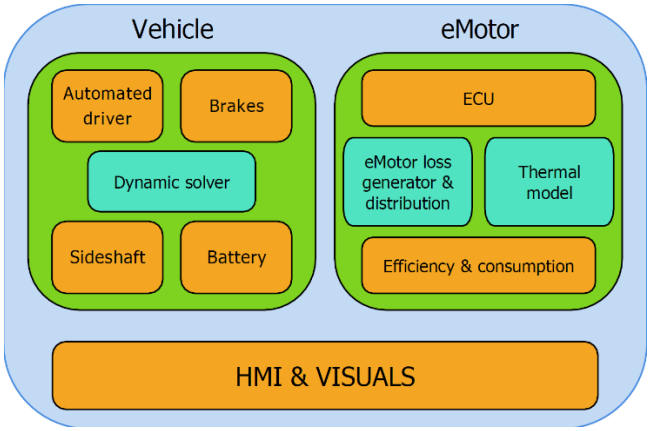


Fig. 7 Components of the simulation environment of the CPTB.

The thermal model consists in a LPTN that describes the heat flows inside the motor and the temperatures of its nodes. This model incorporates an estimator based on an Extended Kalman Filter (EKF) to fuse data from physical sensors into the evaluation of the thermal dynamics.

Additional blocks in the eMotor domain include an efficiency module responsible for the evaluation of the efficiency of the ePowertrain, and an electronic control unit (ECU) that implements a derating strategy to prevent motor overheating in critical situations.

Moreover, a human-machine interface (HMI) and a python-based display have also been implemented to enable the visualization of the temperature status of the motor.

## 2.2 Towards a Digital Twin for eMotors

The eMotor domain in the test bench is the starting point for a digital twin of the DUT, geared towards obtaining high-fidelity information about the operation point of the tested motor beyond the readings of the physical sensors mounted on it.

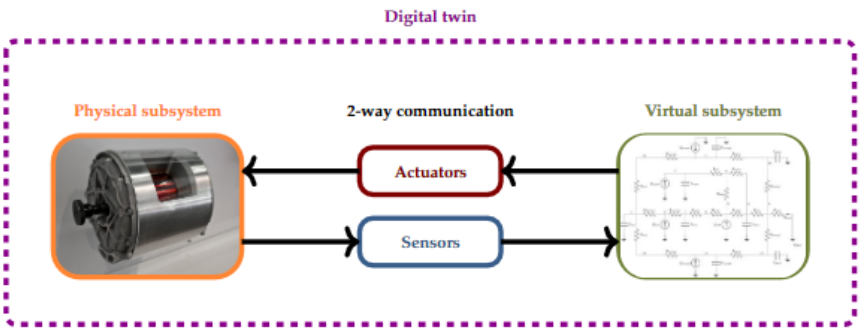


Fig. 8 Illustration of the digital twin concept.

The digital twin concept is illustrated in Figure 8. The physical subsystem under test in the bench, the eMotor in this case, is replicated by a high-fidelity virtual representation, which aims to capture the representative phenomena that take place in its real-world counterpart. A bi-directional communication between the physical and the virtual subsystem is used to convey information about the operation point of the DUT to is computational representation, which in turn provides simulation and analysis results that can be used in decision-making, for instance to determine commands to drive the real ePowertrain [23]. The virtual representation includes a probabilistic treatment of the data gathered from the sensors mounted on the DUT, as well as the results of the simulation conducted in the virtual environment [24]. This information can be used to update the computational model during the life cycle of the eMotor, including for instance the effect of damage suffered by the part, or the aging of materials.

This digital twin of the DUT is currently being developed, but some of its functionality is already operational, in particular the description of thermal phenomena by means of LPTN simulation, and the simulation and sensor data fusion through EKF-based methods. These are described in further detail in Section 4. In this particular application, the thermal observer in the bench was used to provide an estimation of the component temperatures in critical points, at which sensors often cannot be placed in production components. Examples of these locations are the inner part of the eMotor, more specifically the rotor, the magnets, and the central part of the winding. Even in testing facilities, settings sensors in these areas is a highly complex task.Temperature readings from these locations would be very useful to determine the operation point of the motor and to decide on the control strategy adopted to operate it. Indeed, in the winding, when there is a cooling system for the stator assembly extremes, the hot-spot moves into the active winding. In the rotor the hot-spot is mainly located in the center of the stack [25].

Identifying these hot-spots is essential for the definition of derating strategies; the thermal characterization of the eMotor is, accordingly, fundamental to avoid early deterioration or failure. In this context, digital twins can play a central role in the calibration and update of the thermal representation of the eMotor for a wide range of boundary conditions.

## 3 Lumped Parameter Thermal Network Calibration with the CPTB

The thermal circuits used to describe the behavior of the eMotors tested in the bench follow the implementation and solution approaches presented in [26]. LPTNs express the thermal inertia and heat transfer characteristics of a device, as well as its heat generation, by means of lumped components, namely thermal resistors, capacitors, and heat sources, which are similar to the ones used to build electric circuits. Nodes in a LPTN stand for significant locations in the physical component, subjected to a temperature that plays a role similar to a voltage in an electric circuit; the heat that flows between these nodes is analogous to an electric current.

The system thermal dynamics is described by a set of $n$ variables $\mathbf{q}$ that comprises $n_\mathrm{T}$ temperature values and $n_\mathrm{Q}$ heat flows, grouped in terms $\mathbf{q}_\mathrm{T}$ and $\mathbf{q}_\mathrm{Q}$, respectively:

$$\mathbf{q} = [\ \mathbf{q}_\mathrm{T}^\mathrm{T} \quad \mathbf{q}_\mathrm{Q}^\mathrm{T}\ ]^\mathrm{T} \qquad \text{Eq. 1}$$

The system variables $\mathbf{q}$ are not independent and they must satisfy the algebraic constraints imposed by Kirchhoff's laws and the constitutive equations of some components, such as thermal resistors, and heat sources. These constraints can be grouped in an $m$ x 1 term, $\mathbf{\Phi}$

$$\mathbf{\Phi}\ (\mathbf{q}, \mathbf{v}, \mathrm{t}) = \mathbf{0} \qquad \text{Eq. 2}$$

that is a function of time $t$ and the system input $\mathbf{v}$, e.g., fixed temperatures at given nodes and heat generation values. Moreover, thermal capacitors subject the time derivatives of the variables to $p$ linear differential equations in the form

$$\mathbf{\Gamma} = \mathbf{A}\dot{\mathbf{q}} + \mathbf{b}\ = \mathbf{0} \qquad \text{Eq. 3}$$

where $\mathbf{A}$ and $\mathbf{b}$ are $p$ x $n$ and $p$ x 1 terms that depend on the physical properties of the capacitors and the circuit topology.

Equations 2 and 3 can be used to describe the dynamics of any electric or thermal system. The particular features and structure of LPTNs, however, make it possible to write them in the form

$$\begin{bmatrix} \mathbf{\Phi} \\ \mathbf{\Gamma} \end{bmatrix} = \begin{bmatrix} \mathbf{\Phi_q q} + \mathbf{\Phi_v v} \\ \mathbf{A}\dot{\mathbf{q}} + \mathbf{A}_1\mathbf{q} \end{bmatrix} = \mathbf{0} \qquad \text{Eq. 4}$$

where $\mathbf{\Phi_q}$, $\mathbf{\Phi_v}$, and $\mathbf{A}_1$ are $m$ x $n$, $m$ x $r$, and $p$ x $n$ matrices, respectively, with $r$ the number of inputs that act on the circuit.

The matrices in Eq. 4 have a constant structure for each LPTN and their numerical values depend only on the circuit topology and the physical parameters of its components. In order to simulate the dynamics of the thermal system, the nonlinear system of equations in Eq. 4 has to be solved and integrated in the time domain.

The DUT is described by means of a modular LPTN built with the formulation presented in Eqs. 1-4, in which the system topology has been divided into the following areas: shaft, bearings, rotor, magnets, end-plates, end-rings, stator iron, active winding, endwindings, housing with heat extraction sinks, cooling jacket, and internal air cavities. Figure 9 provides an overview of these areas and the heat transmission channels between them. Dashed lines in the figure represent convection between components and fluids, while solid lines denote conduction between parts.

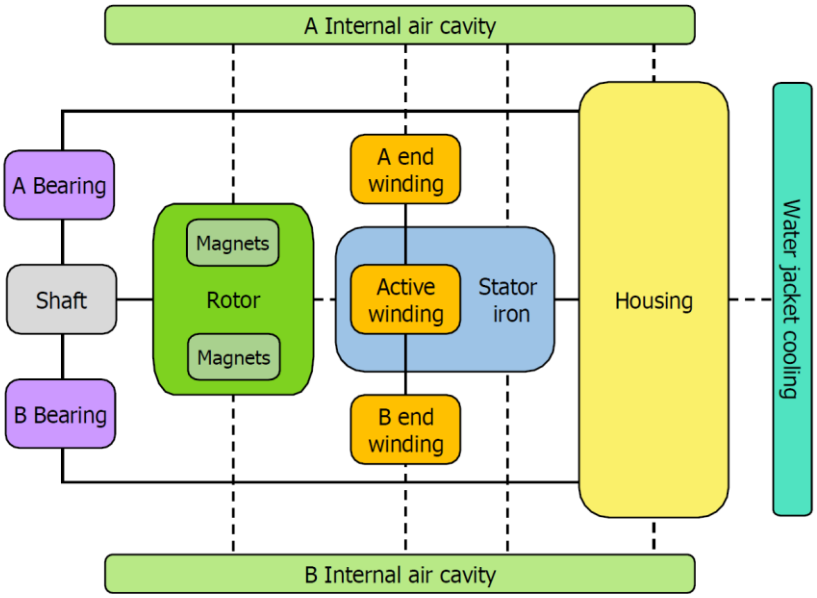


Fig. 9 Thermal sections of the PMSM under study.

The LPTN model was initially formulated as a complex network composed of hundreds of nodes. The computational model of the motor, however, is intended to deliver real-time performance in the test bench; moreover, future applications of the LPTN are likely to be deployed in low-power hardware platforms, such as the ones present in automotive inverters. For these reasons, a reduced 21-node model was developed, merging parameters from the original LPTN while preserving the physical meaning of the scheme. The initial parameters of the system were scaled down from the model of a bigger motor, previously calibrated.

Thermal losses, which are represented in the LPTN by means of heat sources, are the main inputs of the thermal model of the eMotor. Thirteen heat sources were identified: seven in the copper components located in the active winding, endwindings, and the terminal rack; three in the laminated iron components such as the stator teeth, yoke and rotor; one for the magnets and one for each bearing. The losses at the winding copper and the stator iron feature a low variability and can be considered to be accurately known. The magnet losses, conversely, were more difficult to model; these were calculated by means of Finite Element Method (FEM) 2D simulations.

The thermal parameters and inputs of the LPTN used in the CPTB need to accurately match the physical properties of the DUT to deliver correct predictions about its internal temperatures and heat flows. Arriving at correct values of these is often challenging for several reasons. In the first place, LPTNs rely on a simplification of the thermal phenomena that occur in a physical system; this, together with the uncertainties that affect component properties, hinders the direct derivation of thermal parameters from theoretical formulas. An adjustment of the model parameters is always required; often several possible solutions exist to this problem and not all of them are physically meaningful. The difficulty of this adjustment increases proportionally to the number of components and, therefore, the descriptive accuracy of the models.

### 3.1 Calibration protocol

There are many alternatives when trying to identify the parameters of an LPTN model. Depending on the number of nodes and parameters, however, having an efficient method can strongly reduce the computational cost and time of model calibration. Sensitivity analysis is a powerful tool that highlights which parameters are more relevant for the nodes desired, the critical ones. Thus, it allows the selection of the most influential nodes as prioritary in the adjustment process, in order to get to a faithful system description by means of parameter optimization.

Sensitivity analysis is a commonly employed technique for refining strategies, as evidenced by previous works such as [27], [28], and [29]. In the majority of cases, a finite differences methodology is adopted. This involves iteratively subjecting chosen parameters to perturbations and subsequently performing repeated forward-dynamics simulations. This approach yields an estimation of the sensitivity of the system dynamics concerning said parameters. Such estimations prove valuable in identifying pivotal parameters, thereby concentrating optimization efforts on them. However, it is worth noting that the computational demands of finite-difference-based sensitivity analysis increase substantially when dealing with a large number of parameters, as highlighted by [27]. Furthermore, accuracy concerns arise if the selection of perturbation sizes is not judiciously executed, as indicated by [30]. This issue can be mitigated by leveraging the technique of complex-step differentiation, as outlined by [31]. An alternative avenue for assessing system sensitivity involves the utilization of automatic differentiation (AD) methods. These methods rely on the decomposition of computations into elemental mathematical operations possessing established analytical derivatives, as elucidated by [32], [33], and [34].

Within this context, a calibration protocol, as explained in [35], is formulated based on dynamic sensitivity analysis. This protocol entails optimizing the most influential parameters associated with critical nodes in the model according to the tests frequently used in eMotor characterization: continuous service (S1) and peak service (S2) curves. In the first ones, a constant load is applied long enough to attain a thermal equilibrium. For each of the operation points, a constant speed value is administered and the corresponding torque value is chosen to reach 180ºC in the hot spot of the motor after the application of the speed and torque point in a period of about 30 minutes. These cycles represent a maintained speed operation of a vehicle, adequate to capture the steady-state behaviour of the electric machine. In S1 curves, there is also a transient period until thermal equilibrium is achieved, however, it represents a slow dynamic and may not capture the entire thermal inertia spectrum, especially the fastest ones. Indeed, S2 curves are used precisely for this purpose. In peak service tests a torque value is requested during a time frame of 10, 30 or 60 seconds most commonly. Dissimilar to S1 curves, these tests do not reach thermal equilibrium. Actually, these tests terminate when the hot spot reaches the maximum admissible temperature (180ºC) or when the inverter or battery exceed their current limit.

To validate the adequacy of the fitting, the Worldwide harmonized Light vehicles Test Procedure (WLTP) cycle [36] is employed.

Moreover, even if the eMotor was calibrated well at the start of its operation, it's important to note that its thermal properties can change over time due to factors like aging and the wear and tear of critical components from heat cycles or overheating [37]. Some system inputs, such as thermal losses, are subjected to quick variations during operation, and they introduce an additional source of uncertainty in the system representation. It was observed that it is highly complex to obtain an expression that faithfully represents the losses of the magnets in the eMotor.

In the present study, the dynamics equations were differentiated (which were presented in Section 3) with respect to the system parameters to obtain the analytical sensitivity of temperatures and heat fluxes with respect to the critical parameters. Then the resulting most influential resistances and capacitances in the LPTN model were optimized according to S1 and S2 curves, using a Levenberg-Marquardt algorithm. The parameters were constrained to vary plus-minus 300% from their initial values.

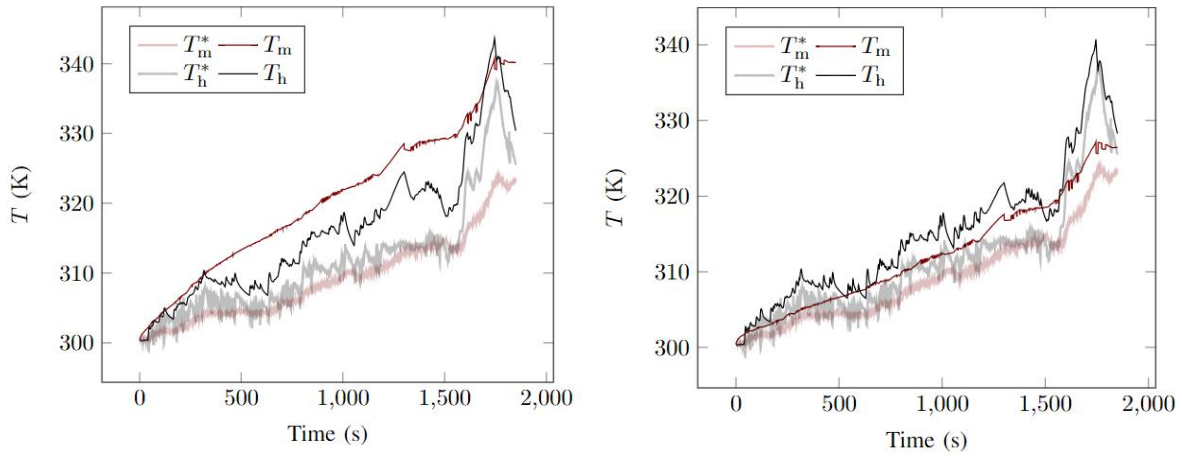


Fig. 10 Temperatures in the PMSM during the WLTP cycle: sensor readings at the magnets and the stator hot spot ($T_m^*$ and $T_h^*$ and optimized LPTN predictions at these locations ($T_m$ and $T_h$)).

Figure 10 shows the comparison between the initial state and the state after the application of the sesitivity analysis presented in the Section 3.1 and the optimization procedure. The capacity to improve the models tuning the most influential parameters demonstrates to be potentially effective and computationally fast compared to other literature methodologies. For instance, when compared to the finite differences method, the time consumed for this other approach is at least proportionally higher to the number of parameters. The LPTN model used for the current investigation counts with around 70 parameters, so the method employing finite differences would be at least 70 times slower computationally speaking [35]. Besides, the usage of the presented method avoids the selection of the perturbation size required by finite difference methods.

## 4 Kalman Filter In-Operation Model Adjustment

Even though an acceptable calibration may have been obtained at the beginning of the operation of the eMotor, its thermal parameters may change over time during operation due to aging and the deterioration of the critical components caused by thermal cycling or overheating [37]. Besides, some system inputs, such as thermal losses, are subjected to quick variations during operation, and they introduce an additional source of uncertainty in the system representation.

Therefore, an EKF is used to handle these problems and arrive at a physically meaningful description of the thermal behaviour of the DUT, following the approach presented in [12]. The EKF allows for the online estimation of the thermal parameters and inputs of the LPTN, as well as the temperatures of the nodes of interest. A conventional KF could be used instead for state estimation, but this would require the thermal parameters and input values to be accurately known during operation.

### 4.1 Input and parameter estimation

The observer is based on the discrete-time Kalman filter, which requires to write the system dynamics equations as

$$\mathbf{x}_{k+1} = \mathbf{F}_k \mathbf{x}_k + \mathbf{G}_k \mathbf{u}_k + \boldsymbol{\omega}_k \quad \text{Eq. 5}$$

Where $\mathbf{x}$ and $\mathbf{u}$ are the system state and inputs, terms $\mathbf{F}$ and $\mathbf{G}$ are the system and input matrices, and $\boldsymbol{\omega}$ is the system noise. Subscripts $k$ and $k+1$ stand for the current and the next time-steps in the representation of the system dynamics. Sensors mounted on the system are used to retrieve an array of measurements $\mathbf{o}$, of size $s$ x 1. The system model can be used to calculate the values of these readings as

$$\mathbf{h}_\mathrm{k} = \mathbf{H}_\mathrm{k} \mathbf{x}_\mathrm{k} + \mathbf{N}_\mathrm{k} \mathbf{u}_\mathrm{k} \quad \text{Eq. 6}$$

where $\mathbf{H}$ and $\mathbf{N}$ are linear combination matrices. The sensor measurements are subjected to noise, which, as it was the case with the system noise, is assumed to be white Gaussian noise.

The discrete Kalman filter provides an estimation of the state and the error covariance $\mathbf{P}$ at time $k+1$, starting with the a priori estimates

$$\hat{\mathbf{x}}_{k+1}^{-} = \mathbf{F}_\mathrm{k} \hat{\mathbf{x}}_k^{+} + \mathbf{G}_\mathrm{k} \mathbf{u}_\mathrm{k} \quad \text{Eq. 7}$$

$$\mathbf{P}_{k+1}^{-} = \mathbf{F}_k \mathbf{P}_k^{+} \mathbf{F}_k^{\mathrm{T}} + \mathbf{Q} \quad \text{Eq. 8}$$

where $\hat{\mathbf{x}}_k^{+}$ and $\mathbf{P}_k^{+}$ are the a posteriori estimated state and covariance matrix at step $k$, and $\mathbf{Q}$ is the noise covariance matrix of the system. A correction step delivers the a posteriori values of these terms:

$$\hat{\mathbf{x}}_{k+1}^{+} = \hat{\mathbf{x}}_{k+1}^{-} + \mathbf{K}_{k+1}(\mathbf{o}_{k+1} - \mathbf{h}_{k+1}) \quad \text{Eq. 9}$$

$$\mathbf{P}_{k+1}^{+} = (\mathbf{I} - \mathbf{K}_{k+1}\mathbf{H}_{k+1})\mathbf{P}_{k+1}^{-} \quad \text{Eq. 10}$$

where $\mathbf{I}$ is the identity matrix and $\mathbf{K}$ is the Kalman gain, evaluated as

$$\mathbf{K}_{k+1} = \mathbf{P}_{k+1}^{-}\,\mathbf{H}_{k+1}^{\mathrm{T}}(\mathbf{H}_{k+1}\,\mathbf{P}_{k+1}^{-}\,\mathbf{H}_{k+1}^{\mathrm{T}} + \mathbf{R})^{-1} \quad \text{Eq. 11}$$

where $\mathbf{R}$ is the covariance matrix of the measurements. In order to use Eqs.5-10 in the estimation of state, inputs, and parameters of LPTNs, it is necessary first to express the system dynamics in Eq. 4 in terms of an independent set of coordinates. This can be achieved extracting a reduced subset of $p$ variables $\mathbf{z}$ using a constant $p$ x $n$ matrix $\mathbf{B}_0$,

$$\mathbf{z} = \mathbf{B}_0\mathbf{q} \quad \text{Eq. 12}$$

The EKF used for input and parameter estimation includes the $p$ independent variables $\mathbf{z}$, their derivatives with respect to time, $\dot{\mathbf{z}}$, and the set of $o$ parameters $\boldsymbol{\rho}$ that need to be estimated, in its extended state term of size $(2p + o)$ x 1; the filter inputs $\mathbf{u}$ include the $r$ system inputs $\mathbf{v}$ and their derivatives with respect to time:

$$\mathbf{x} = \begin{bmatrix} \mathbf{z} \\ \dot{\mathbf{z}} \\ \boldsymbol{\rho} \end{bmatrix}; \qquad \mathbf{u} = \begin{bmatrix} \mathbf{v} \\ \dot{\mathbf{v}} \end{bmatrix} \quad \text{Eq. 13}$$

The state variables in Eq. 13 must satisfy Eq. 3; this condition is imposed following the perfect measurements approach [38]. The details of these derivations can be found in [12]. It must be noted that the correct behaviour of the estimation algorithm presented in this section requires that the system dynamics is almost linear during the time-step $[k, k+1]$. To keep this assumption valid, the value of $\tau$ has to be selected appropriately to match the dynamics of the thermal effects here described.

### 4.2 Results

The best way to test the method was to determine its performance during a duty cycle, with the intention to estimate the losses of the most uncertain heat sources in the thermal model of the digital twin. The tested motor was subjected to a series of three WLTP cycles in the CPTB described in Section 2. This common homologation test was selected because of its coverage of a wide range of motor speeds, as it includes four consecutive low, medium, high and extra high velocity segments [36].

The inputs to the algorithm are the heat sources, parameter values and measurements retrieved from testing in the selected duty cycle. During the experiments, four readings were retrieved from temperature sensors located at the external surface of the rotor, the magnets, and the A-side and B-side endwindings. In this case, only these measurements were significative according to the nodes in the LPTN model. Results from a single test run are shown because of the low variability of the recorded cycles. Otherwise, the output of this particular application is the estimated value for magnet losses, which have been proved to be the most uncertain heat source to the system.

Preliminary tests showed that the values of the thermal losses had the greatest impact on the correctness of the temperature predictions of the eMotor model. Accordingly, for each experiment, the thermal dynamics of the DUT was evaluated twice. First, the thermal behaviour of the system was simulated using the 21-node LPTN described in Section 3 using analytical expressions of the thermal losses in the DUT. The simulation was carried out solving the nonlinear system of equations 4 through Newton-Raphson iteration and using a second order Backward Differentiation Formula (BDF2) as numerical integrator. Next, the same LPTN model was combined with the EKF-based observer described in the previous section to carry out the correction of the uncertain thermal losses, which are system inputs from the point of view of the formulation in previous section.

In these procedures, the readings from the rotor and endwindings thermocouples were treated as sensor measurements for the estimation algorithm (they were included in array $\mathbf{o}$), while the temperature readings from the magnets were used for verification only, to determine the level of accuracy attained by the estimation process. The numerical simulation and estimation were performed using a sample time $\tau = 0.5$ s.

To sum up, the heat losses at the magnets are the input corrected by the estimation algorithm; the sensor measurements obtained from the bench are the temperatures at the A and B endwindings and the outer diameter of the rotor core. The temperature at the magnets is measured and used as validation variable, but not used in the input estimation.

The values delivered by the estimation algorithm are compared to the uncorrected forward-dynamics simulation of the the thermal dynamics of the system in Figures 11-13.

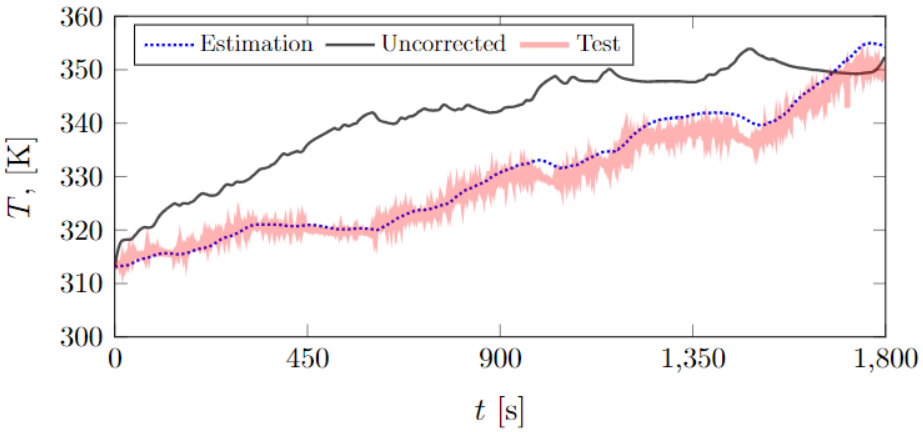


Fig. 11 Magnet temperature in the WLTP cycle.

Figure 11 shows the time-histories of the magnet temperatures obtained with the uncorrected LPTN simulation and the estimation algorithm, and compares them to the thermocouple measurements at the same location. The estimation procedure brought the maximum absolute error in the magnet temperature in this scenario down to 6 ºC, with a mean absolute error below 1.6 ºC. Figure 11 confirms that the incorrect adjustment of the LPTN model introduces errors in the prediction of the temperature of

the critical hot-spots of the system, rendering the uncorrected simulation results unreliable. These errors were largely removed by the use of the input observer.

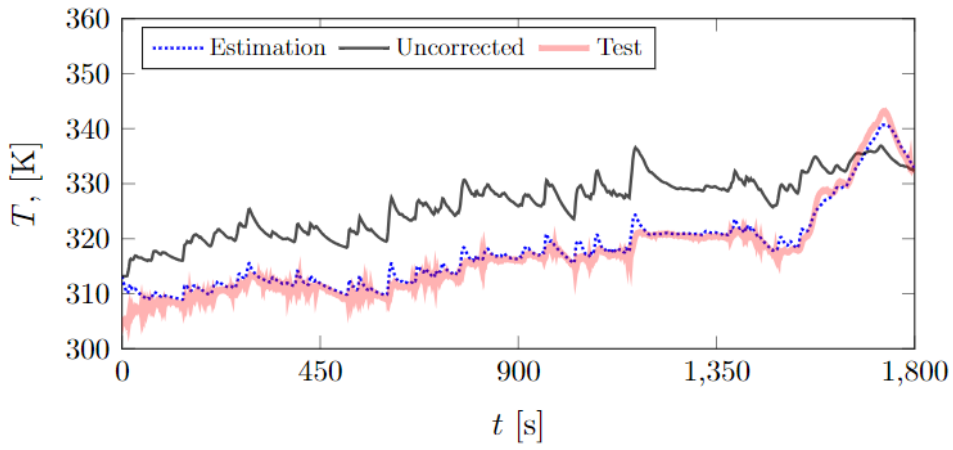


Fig. 12 A-side endwinding temperature in the WLTP cycle.

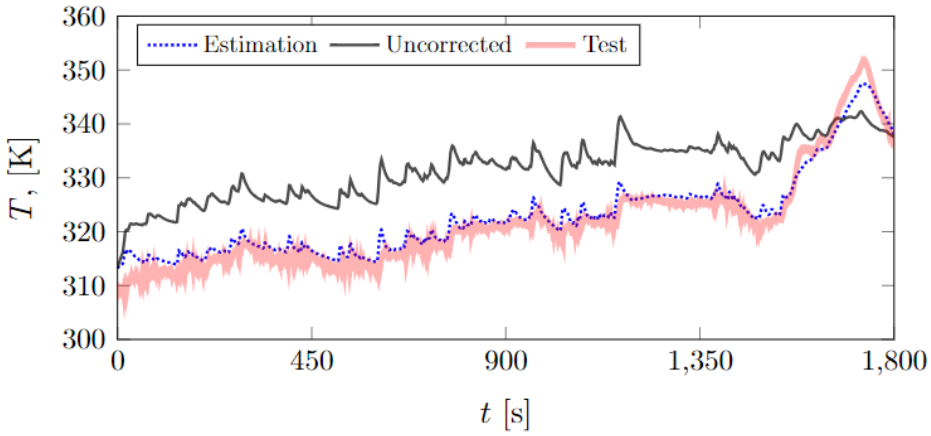


Fig. 13 B-side endwinding temperature in the WLTP cycle.

Figure 12 shows the temperature of the A-side endwinding in the WLTP cycle. The uncorrected LPTN simulation curve overestimates the node temperature, except in the extra-high velocity stretch (between t = 1400 s and t = 1800 s), in which the uncorrected simulation fails to capture the expected increase in temperature. The estimation approach corrects these deviations. Relatively small overshoots can be observed in the system response, which could be related to the signal noise; additionally, the peak temperature predicted is a few degrees below the experimentally measured values. In spite of these issues, the estimation results represent an improvement over the uncorrected simulation ones. A similar behaviour can be observed in Fig. 13, which contains data for the B-side endwinding.

In the latter two cases, the maximum differences between the temperature estimated at a node and the corresponding sensor measurements were below 8 ºC, with a mean absolute error below 2 ºC.

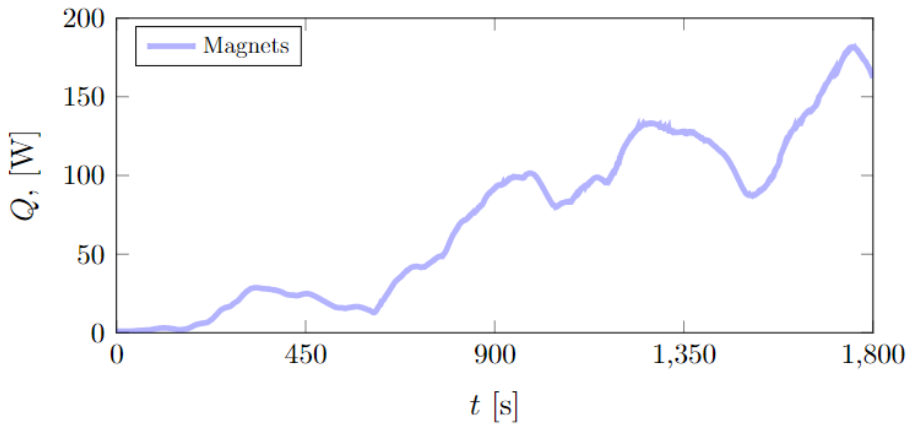


Fig. 14 Magnet heat source estimation result for the WLTP cycle.

Figure 14 contains the magnet heat losses, i.e., the input adjusted by the observer, delivered by the estimation algorithm in this scenario.

The results obtained in the WLTP cycle support the ability of the proposed estimation method to correct LPTN simulation results by means of sensor data fusion. Results also confirmed that the estimation algorithm was able to deal with the measurement noise introduced by the telemetry data acquisition in the readings from the thermocouples. It must be pointed out, however, that the estimation seems to introduce a small delay in the thermal response of the system, in particular in periods in which the magnet temperature decreases.

## 5 Thermal Ageing Effects on an Automotive Grade Motor Stator

The function of the insulation in the stator of electric machines is to both insulate electrically the winding from the laminated steel core and enhance the conduction of the heat generated from the conductors, which are the main heat sources, towards the laminated steel to be disipated by the cooling systems. Generally, these can be a water jacket or any type of oil cooling system. Insulation systems also grant higher structural rigidity to the conductors in the slot.

The eMotor, and so the insulation system, is usually subjected to thermal cycling, thermal shock, exposure to high temperatures and partial discharge phenomena during the performance of the machine.

These effects produce the deterioration of the materials that form the insulation conglomerate; in the case of the DUT these materials are:

1. Hairpin individual conductor organic enamel (polyester-imide, over-coated with polyimide-amide);
2. Epoxy resin impregnation.
3. Single-layered Nomex® paper, which can be double-layered in some areas depending on their configuration.

In the present investigation, the thermal ageing accumulation was studied. It is essential to have a very accurate calibration of the so-called critical parameters [39]-[41]: the correct approach on the heat extraction paths and convection heat transfer coefficients, interference resistance between stator and housing, thermal capacities and thermal conductivities of the materials, especially in multi-material conglomerates such as the insulation system [27].

Indeed, most of the LPTN models in the literature do not take into consideration that some of these parameters could dynamically vary due to ageing. Hence, the models are static in time and it could lead, potentially, to erroneous results. More specifically, it has been shown in wire conductor motorettes that the equivalent conduction resistance representing the insulation between the winding and the stator in the active part of the machine present variations above 10 ºC when subjected to thermal ageing at 230 ºC for more than 200h [19]. Therefore, it is concluded that the thermal conductivity of the insulation conglomerate increases with thermal ageing, gradually worsening the heat conductivity and extraction from the windings, the core of the heat sources.

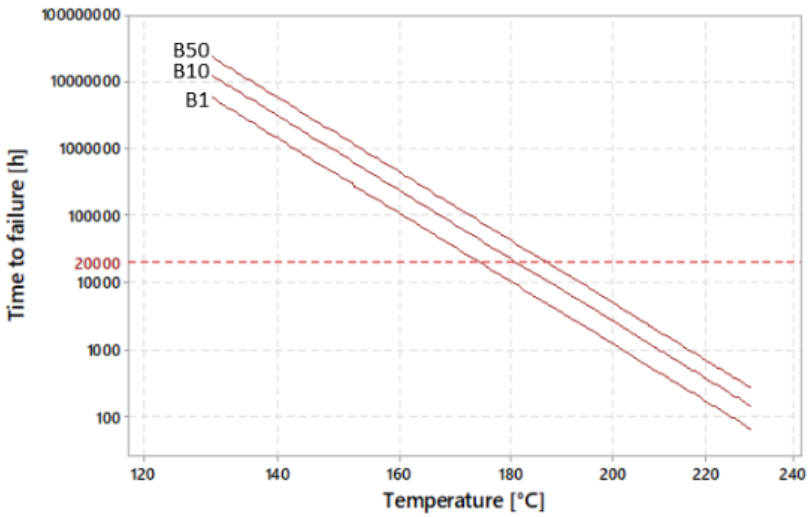


Fig. 15 Thermal endurance plot (Arrhenius curve) for class-H insulation systems [42].

Based on the thermal endurance plots (or Arrhenius curves) shown in Figure 15, a failure time as a funcion of the ageing temperature and the failure probability can be estimated. While it would be unfeasible to replicate a failure at 180ºC for timing reasons (20000 hours), the curves allow to perform the heating at higher temperatures, being able to escalate the law of deterioration obtained [42].

However, this has been applied to wire conductor motorettes, not to automotive-grade stators. It is of interest to validate these effects and to obtain a rule of deterioration for the stator insulation for complete machines. In Section 5.1 the experiments that were carried out for the present investigation are described, as well as the results obtained.

### 5.1 Experimental campaign

An experimental campaign was conducted to thermally age an automotive-grade stator and its insulation system. A stator consisting of laminated steel core, haripin winding and enamel-epoxy-Nomex® insulation system was selected for the study. A particularity of the eMotor employed is that it has 6 conductors.

Figure 16 presents the setup used for the experiments. The stator was placed on a glass-fiber support making the minimum possible contact. A direct current (DC) source was connected to two of the three phases that are instrumented, entering and exiting from a different phase and leaving one phase wihtout current. Finally, a datalogger was used to retrieve all the data coming from the sensors located in the stator. Simultaneously, the temperatures were measured with a thermographic camera to capture any effects unseen in the sensors.

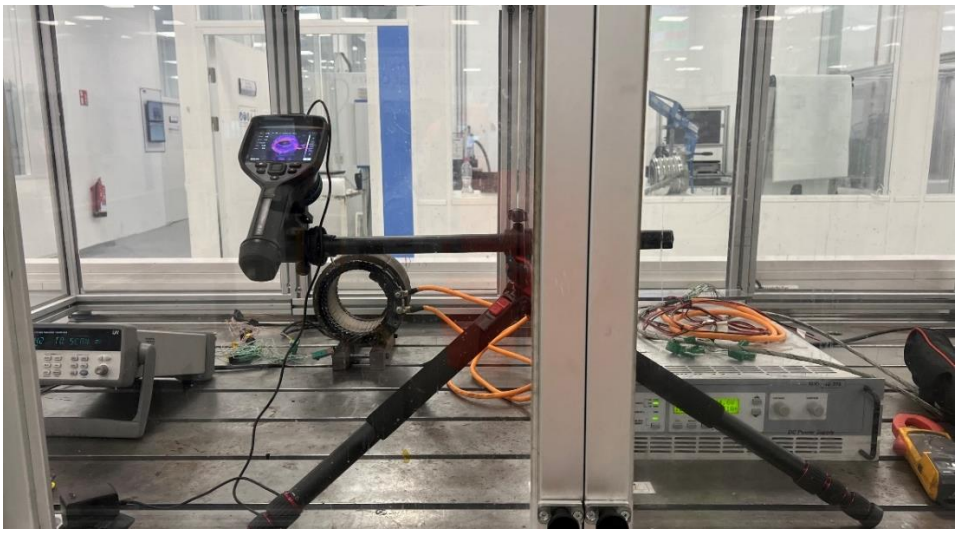

Fig. 16 Test setup for ageing measurements.

Firstly, a series of variability measurements were carried out to ensure the repeatability of the measurements under practically identical conditions. This test was conducted introducing 160 A to two of the phases of the eMotor until the steady state temperature was achieved. As the variability was under 3%, the setup was validated for further tests.

Secondly, the iterative procedure applied was a heating cycle in the oven at 230 ºC for 12 hours, an electrical insulation check and a DC current application of 160 A until steady state temperatures were achieved in the setup described and under practically identical conditions. In total 21 heating cycles under these conditions were performed, 20 of 12 hours and a last one of 60 hours, with their corresponding DC current application until steady-state temperature was achieved in the motor. The data of all the thermocouples was acquired and saved for comparison. For this purpose, six thermocouples were installed in each of the winding heads. Figure 17 presents the distribution of these sensors, being most of them in the space between the most inner layers of conductors and circumferencially distributed.

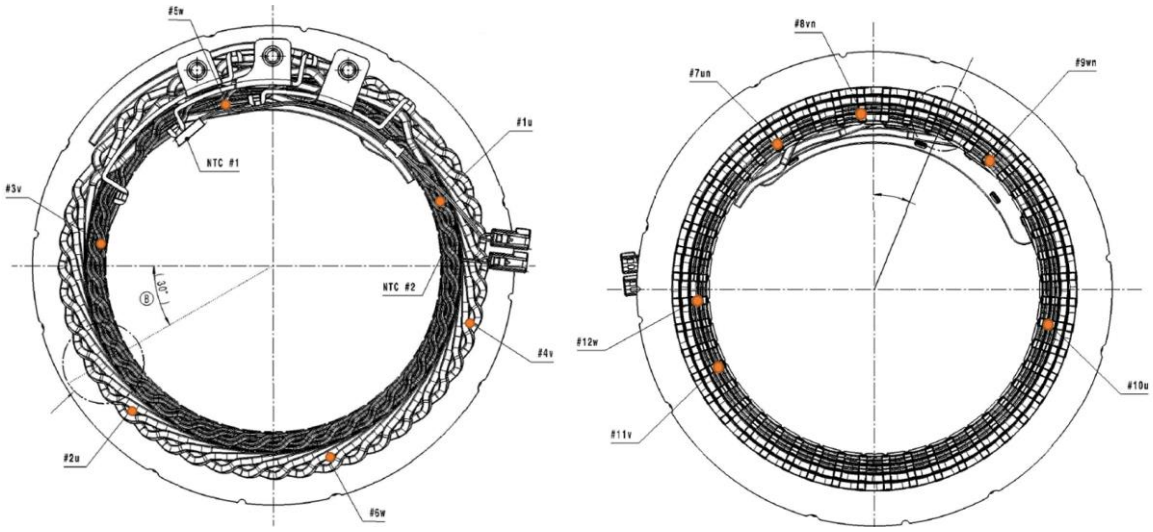


Fig. 17 Thermocouple locations in the stator of the eMotor employed for ageing tests.

Figure 18 presents the maximum temperature read in the stator in steady-state conditions on each of the experiment iterations. In all the cycles, the aforementioned sensor is *3v,* located in the winding head upper area (see Figure 17).

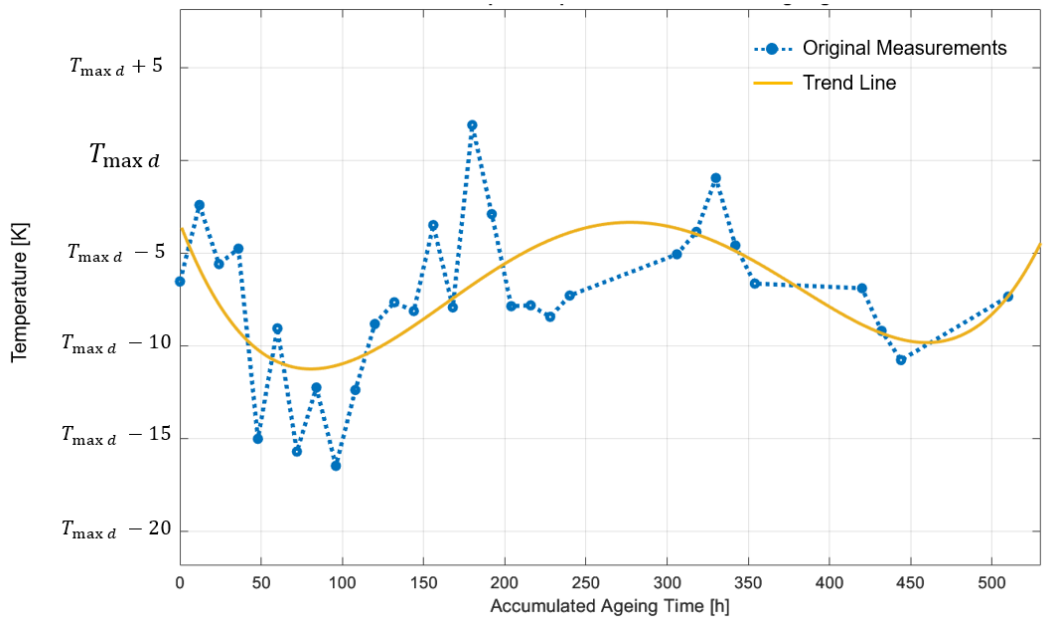


Fig. 18 Hot spot temperature evolution results after applying DC current until steady-state temperature after 29 heating cycles.

During the experiments, after the first eight 12 hour cycles a decrease in the hot spot temperature in the steady state was recorded with some up and downs. This was not expected, as in the state of the art [37] a clear upwards tendency in the hot spot temperature was observed from the beginning of the tests, having around a 30% of equivalent conductivity decrease by the first 24 hours of ageing and almost a 50% decrease by approximately 300 hours. However, from the ninth cycle to the fifteenth included, the hot spot temperature increased with minor variations until the initial steady state temperatue is surpassed. In the last six cycles though, the upwards

tendency was not followed. Hence, it is observed that isolated thermal cycling can increase the steady state temperature not only for motorettes as presented in [19] but also for automotive-grade electric motors, but more experiments need to be carried out to confirm the tendency from the experimental campaign and its repeatability.

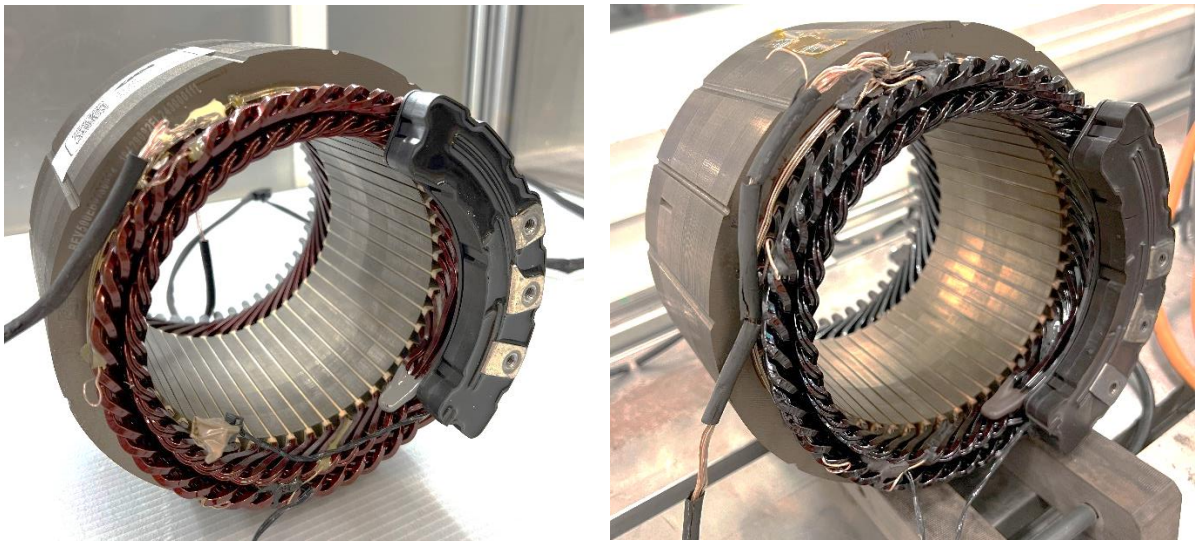

Fig. 19 Stator before (left) and after (right) the thermal ageing experimental campaign.

As shown in figure 19, the deterioration of the stator was very evident, but within the cycles performed it was not corresponded by the response of the hot spot temperature evolution after thermal cycling according to the literature. All epoxy resins look much darker and seem to have been melted. The enamel as well looks dark but shows no cracks, neither do the epoxy on the welded conductors. The paper also presents a brownish color but no cracks and in the active part the extremes also look progressively browner into the middle where it is less affected. In general, the visual appearance indicates a more aged state than the demonstrated in the recorded steady state temperatures.

The stator insulation system was expected to be much more deteriorated as shown in the work of Madonna et al. [19], [37], [41], [42], nervertheless, it did not behave just as what it was presented in the literature. This could be due to the change from a flat and shorter motorette to an axially longer and circular geometry as an automotive-grade stator has. It is interesting how the performance improves, resulting in lower steady state hot spot temperatures, which was opposed to the expected effect. Indeed, not only that but it took much longer than expected based on literature to see an increase in the hot spot temperature in cycle 15, even if in the next cycle it went down again. As a conclusion, the tendency for the time being is still uncertain and more thermal cycles and DC current applications will be performed in order to reach to the failure point.

### 5.2 Model Update Including Thermal Ageing Effects

Nowadays, for its complexity, the LPTN models are static and are not modified, leading to either power loss for excessive heating due to component degradation or to overheating deriving ageing acceleration.

Based on experimental results this effect can be implemented in thermal models to predictively obtain the ageing state of the insulation system due to the exposure to high temperatures. The aim of this investigation is to obtain a rule of deterioration that could be applied to update the stator insulation equivalent conductivity as a function of time above the threshold temperature for the insulation class of the system. Equivalent condutivity is defined as the amalgam conductivity of enamel, epoxy resin and Nomex® of the insulation system.

A series of CFD simulations will be carried out to obtain the equivalent conductivity values that match the hot spot temperatues observed in the study as in [19]. Those values will conform the law of thermal degradation of the stator insulation for 230 ºC heating cycles. However, thanks to the Arrhenius curves, and for the same failure probability, the law can be adapted to 180 ºC heatings, which is the temperature limit for the present stator, with a class-H winding insulation. Based on this law and by means of a state observer, the conductivities of the active winding resistances can be updated as a function of the accumulative heating above 180 ºC in the eMotor. Thus, the parameters of the model adapt as the eMotor deteriorates with time.

For a more accurate approach, other effects as thermal shock and partial discharge phenomena should be taken into account and applied. The more complete, the more faithful the thermal digital twin law of deterioration will be. Taking into account all the ageing effects, the implementation of such law will enable to have a realistic motor ageing model.

## 6 Conclusions and Future Work

In this study, first of all, a CPTB has been described, as a platform for automotive-grade electric motor digital twins. Based on a simplified LPTN model of the eMotor, secondly, the results of a calibration protocol driven by a novel sensitivity analysis method have been shown, demonstrating an efficient method to calibrate the most influential parameters with respect to the selected temperature nodes. The parameters were optimized according to the motor characterization curves S1 and S2 and the improvement was verified in the WLTP cycle. With this method, the mean absolute error decreased 3ºC for the endwinding hot spot and circa 10ºC for the magnets. Then, an estimation method has been presented, used to reduce the uncertainty in the losses of the magnets to adjust the same LPTN model. Here, by the estimation of the magnet heat source with an EKF, the mean absolute error of the magnet temperature in the model decreased from 6ºC to below 2ºC. The combination of both methods could potentially be part of a complete calibration protocol where uncertain heat sources and parameters could be adjusted for thermal behaviour faithful representation. Finally, an experimental campaign for eMotor stator insulation systems was carried out, aiming to derive an equivalent conductivity decrease law to be implemented in the thermal models to go forward towards eMotor digital twins. The results of the tests do not align with the literature and further work will be conducted to obtain clearer conclusions.

The aim of this investigation is to develop the platform and methods to calibrate and update thermal models for digital twins of ePowertrain motors. In this paper, a CPTB was selected as test platform. This kind of test bench enables the simultaneous operation of a real eMotor and its digital twin, for instance to gain insight into its thermal behaviour; moreover, it makes it possible to interact with a large set of real-time realistic scenarios in a straightforward way, e.g., by means of interaction with a virtual vehicle model. The heart of the digital twin is a LPTN model built based on the original geometry and physical properties of the motor. An electromagnetic model generates the thermal losses to be inputted in the heat sources. However, no matter how accurately the conduction and convection resistances and capacitances, it is fundamental to calibrate the models with experimental data to search for a precise representation of the thermal behaviour of the system.

Under the vision of MBST, and based on the experience of model calibration, CPTBs could very efficiently enable the calibration of models in a semi-automatic manner. Relying on the presented methods such as dynamic sensitivity analysis, most relevant parameter optimization and Kalman filtering, the digital twin could be adjusted and updated. In this work some of the methods and procedures have been shown and their benefits compared to other methodologies existing in the literature. In terms of model calibration, the aim is to introduce a blank template, built based on the different stator and rotor topologies, in the CPTB. Then a sensitivity analysis is run during the execution of a WLTP cycle and the most relevant parameters are selected for optimization in S1 and S2 curves at different temperature levels and cooling conditions. The tests can be run automatically in the test bench, providing the necessary data to launch the offline optimization process. Finally, one or two duty cycles would be launched supported by online heat loss distribution calibration with a Kalman filter. The output of the test would be the adjusted LPTN model, within the admissible limits for the winding hot spot and magnet hot spot nodes and having faithful temperatures for the other nodes in the model too.

Nevertheless, there are some points that need to be further developed in the future, focusing in the CPTB and its methods. Firstly, we expect to explore different Kalman filter approaches for the estimation of the most uncertain losses. In the present work, an EKF has been used, but it would be interesting to analyze the performance of an Unscented Kalman Filter (UKF) to perform the estimation tasks. These are widely used in the field of multibody system dynamics simulation. Secondly, although S1 and S2 curves and the WLTP cycle are usually the tests used for eMotor characterization, it remains as future work to explore the optimal definition of tests that could help characterize and calibrate the LPTN models for digital twins, as well as the most appropriate number of operation points needed to comprehend as much as possible the whole range of operation of the eMotor and so to build a precise and faithful digital twin. Thirdly, albeit the LPTN model has been built iteratively reducing a very detailed model, there is future work to do in the definition of the optimal circuit to represent heat distribution and disipation paths in the eMotor. Specific work on oil cooling models and different topologies' HTCs are planned to be developed in the future, which will require intensive experimental campaigns to accurately explore all the phenomena given in oil cooled motors. In relation with the LPTN model, there will be future investigation in the

field of electromagnetic losses, in order to diminish the uncertainty in the distribution of the magnet losses and iron losses in the stator and rotor, also driven by intensive experimental campaigns.

In the topic of automotive-grade motor insulation ageing, there is great room for future work as well. In the first place, the tests should be redone to analyze the repeatability of the deterioration tendency in the automotive-grade stator evaluated. In the end, a complete stator introduces a much greater level of complexity than the motorettes prsented in the state of the art and opens the door to many circunferential or axial phenomena that could not be identified so far. Secondly, it would be of great interest to couple more ageing effects, in order to have a much more complete model describing how the insulation deteriorates also depending on greater gradient thermal shocks or partial discharge phenomenon. Currently, work in the investigation of partial discharge effects is being conducted.

All these steps will enable the procurement of gradually increasing faithful models for the construction of digital twins of ePowertrain motors. When obtained, and even in previous steps, the cost of testing, decreasing the number of tests, destructive test prototypes will be potentially reduced and, under the MBST vision, the need of physical sensors in the driving units in a vehicle too. Some first advances in this work-line are presented in this investigation.

## 7 Abbreviations

| | |
|---|---|
| BDF2 | 2nd order Backward Differentiation Formula |
| CPTB | Cyber-Physical Test Bench |
| DUT | Device Under Test |
| ECU | Electronic Control Unit |
| EKF | Extended Kalman Filter |
| MBST | Model-Based System Testing |
| PMSM | Permanent-Magnet Synchronous Motors |
| SiTL | System-in-the-Loop |
| S1 | Continuous Service Curves |
| S2 | Peak Service Curves |
| UKF | Unscented Kalman Filter |
| WLTP | Worldwide harmonized Light vehicles Test Procedure |

## 8 References

[1] M. Helmle, B. Müller, F. Von Zeppelin, and F. Hauler, 2015.
Challenges and concepts for the validation of highly automated driving.
Autonomous Vehicle Test & Development Symposium, Stuttgart, Germany.

[2] F. L. Marques dos Santos, R. Pastorino, B. Peeters, C. Faria, W. Desmet, L. C. Sandoval Góes, and H. Van Der Auweraer, 2016.
Model Based System Testing: Bringing testing and simulation close together.
Structural Health Monitoring, Damage Detection & Mechatronics.
Springer, A. Wicks and C. Niezrecki (Eds.).
Volume 7, Pages 91-97
DOI: 10.1007/978-3-319-29956-3_10

[3] S. Glumac, N. Varga, F. Raos, and Z. Kovačić, 2022
Co-simulation perspective on evaluating the simulation with the engine test bench in the loop.
Automatika, Volume 63, Number 2, pages 275-287.
DOI: 10.1080/00051144.2022.2031537

[4] F. Cremona, M. Lohstroh, D. Broman, E. A. Lee, M. Masin, and S. Tripakis, 2017
Hybrid co-simulation: it's about time.
Software & Systems Modeling, Volume 18, Number 3, pages 1655-1679.
DOI: 10.1007/s10270-017-0633-6

[5] N. Tsokanas, R. Pastorino, and B. Stojadinović, 2022.
Adaptive model predictive control for actuation dynamics compensation in real-time hybrid simulation.
Mechanism and Machine Theory, Volume 172, article 104817.
DOI: 10.1016/j.mechmachtheory.2022.104817

[6] S. Sadjina, L. T. Kyllingstad, S. Skjong, and Eilif Pedersen, 2017.
Energy conservation and power bonds in co-simulations: non-iterative adaptive step size control and error estimation.
Engineering with Computers,Volume 33, Number 3, pages 607-620.
DOI: 10.1007/s00366-016-0492-8

[7] B. Rodríguez, A. J. Rodríguez, B. Sputh, R. Pastorino, M. Á.Naya, and F. González, 2022
Energy-based monitoring and correction to enhance the accuracy and stability of explicit co-simulation.
Multibody System Dynamics, Volume 55, Number 1-2, pages 103-136.
DOI: 10.1007/s11044-022-09812-5

[8] G. Stettinger, M. Benedikt, M. Tranninger, M. Horn, and J.Zehetner, 2017
Recursive FIR-filter design for fault-tolerant real-time co-simulation.
25th Mediterranean Conference on Control and Automation (MED), Valletta, Malta, 2017, pages 461-466.
DOI: 10.1109/MED.2017.7984160

[9] B. H. Sputh, L. Thielemans, J. Pašič, C. Ganier, and R. Pastorino, 2021
Model-based real-time testing of fail-safe behavior for in-wheel motor propulsion systems.
IEEE Vehicle Power and Propulsion Conference (VPPC), Gijón, Spain, 2021.
DOI: 10.1109/vppc53923.2021.9699304

[10] D. E. Gaona Erazo, O. Wallscheid, and J. Bocker, 2020
Improved fusion of permanent magnet temperature estimation techniques for synchronous motors using a Kalman filter.
IEEE Transactions on Industrial Electronics, Volume 67, Number 3, pages 1708-1717.
DOI: 10.1109/tie.2019.2905817

[11] S. Jaiswal, E. Sanjurjo, J. Cuadrado, J. Sopanen, and A. Mikkola, 2022
State estimator based on an indirect Kalman filter for a hydraulically actuated multibody system.
Multibody System Dynamics, Volume 54, Number 4, pages 373-398.
DOI: 10.1007/s11044-022-09814-3

[12] B. Rodríguez, E. Sanjurjo, M. Tranchero, C. Romano, and F.González, 2021
Thermal parameter and state estimation for digital twins of e-powertrain components.
IEEE Access, Volume 9, pages 97384-97400.
DOI: 10.1109/access.2021.3094312

[13] T. J. E. Miller, M.I. McGilp, and K.W. Klontz, 2009
Approximate methods for calculating rotor losses in permanent-magnet brushless machines.
IEEE International Electric Machines and Drives Conference, Miami, FL, USA, 2009.
DOI: 10.1109/iemdc.2009.5075175

[14] D. M. Ionel, M. Popescu, M. I. McGilp, T. J. E. Miller, S. J. Dellinger, and R. J. Heideman, 2007
Computation of core losses in electrical machines using improved models for laminated steel.
IEEE Transactions on Industry Applications, Volume 43, Number 6, pages 1554-1564. DOI: 10.1109/TIA.2007.908159

[15] A. Tikadar, D. Johnston, N. Kumar, Y. Joshi, and S. Kumar, 2020
Comparison of electro-thermal performance of advanced cooling techniques for electric vehicle motors.
Applied Thermal Engineering, Volume 183, Part 2, article 116182.
DOI: 10.1016/j.applthermaleng.2020.116182

[16] A. Artacho López, D. J. B. Smith, and B. Mecrow, 2022
Magnet loss reduction: A new technique beyond segmentation and shielding.
11th International Conference on Power Electronics, Machines and Drives (PEMD 2022), Newcastle, UK.
DOI: 10.1049/icp.2022.1045

[17] P. Milanfar and J.H. Lang, 1996
Monitoring the thermal condition of permanent-magnet synchronous motors.
IEEE Transactions on Aerospace and Electronic Systems, Volume 32, Number 4, pages 1421-1429.
DOI: 10.1109/7.543863

[18] A. Boglietti, A. Cavagnino, D. Staton, M. Shanel, M. Mueller, and C. Mejuto, 2009
Evolution and modern approaches for thermal analysis of electrical machines.
IEEE Transactions on Industrial Electronics, Volume 56, Number 3, pages 871-882.
DOI: 10.1109/TIE.2008.2011622

[19] V. Madonna, P. Giangrande, and M. Galea, 2020
On the capability of heat dissipation in thermally aged electrical machines.
2020 International Conference on Electrical Machines (ICEM), Gothenburg, Sweden.
DOI: 10.1109/icem49940.2020.9270744

[20] M. A. Eleffendi and C. M. Johnson, 2016
Application of Kalman filter to estimate junction temperature in IGBT power modules.
IEEE Transactions on Power Electronics, Volume 31, Number 2, pages 1576-1587.
DOI: 10.1109/TPEL.2015.2418711

[21] Oliver Wallscheid and Joachim Böcker, 2017
Fusion of direct and indirect temperature estimation techniques for permanent magnet synchronous motors.
2017 IEEE International Electric Machines and Drives Conference (IEMDC), Miami, FL, USA.
DOI: 10.1109/IEMDC.2017.8002038

[22] E. V. Beyerleyn and P. V. Tyuteva, 2014
Energy efficiency of back-to-back method for induction traction motors testing.
2014 15th International Conference of Young Specialists on Micro/Nanotechnologies and Electron Devices (EDM), Novosibirsk, Russia.
DOI: 10.1109/edm.2014.6882547

[23] M. Grieves and J. Vickers, 2016
Digital Twin: Mitigating unpredictable, undesirable emergent behavior in complex systems, Transdisciplinary Perspectives on Complex Systems, Pages 85-113.
F.-J.Kahlen, S. Flumerfelt, and A. Alves (Eds.), Springer International Publishing
DOI: 10.1007/978-3-319-38756-7_4

[24] M. Shafto, M. Conroy, R. Doyle, E. Glaessgen, C. Kemp, J. LeMoigne, and L. Wang, 2010
(DRAFT) Modeling, simulation, information technology and processing roadmap.
NASA

[25] D. J. B. Smith, 2014
High speed high power electrical machines.
PhD Thesis, Newcastle University.
URL: http://theses.ncl.ac.uk/jspui/handle/10443/2645

[26] B. Rodríguez, F. González, M. Á. Naya, and J. Cuadrado, 2020
Assessment of methods for the real-time simulation of electronic and thermal circuits.
Energies, Volume 13, Number 6, pages 1354.
DOI: 10.3390/en13061354

[27] G. G. Guemo, P. Chantrenne, and J. Jac, 2013
Parameter identification of a lumped parameter thermal model for a permanent magnet sychronous machine.
2013 International Electric Machines & Drives Conference, Chicago IL, USA.
DOI: 10.1109/iemdc.2013.6556329

[28] B. Assaad, K. El kadri Benkara, S. Vivier, G. Friedrich, and Antoine Michon, 2017
Thermal design optimization of electric machines using a global sensitivity analysis.
IEEE Transactions on Industry Applications, Volume 53, pages 5365-5372.
DOI: 10.1109/TIA.2017.2746015

[29] F. Zhang, D. Gerada, Z. Xu, H. Zhang, and C. Gerada, 2019
Sensitivity analysis of machine components thermal properties effects on winding temperature.
22nd International Conference on Electrical Machines and Systems ICEMS, Harbin, China.
DOI: 10.1109/icems.2019.8922095

[30] D. Dopico, Y. Zhu, A. Sandu, and C. Sandu, 2014
Direct and adjoint sensitivity analysis of ordinary differential equation multibody formulations.
Journal of Computational and Nonlinear Dynamics, Volume 10, Number 1, ASME International.
DOI: 10.1115/1.4026492

[31] J. R. R. A. Martins, P. Sturdza, and J. J. Alonso, 2003
The complex-step derivative approximation.
ACM Transactions on Mathematical Software, Volume 29, Number 3, pages 245-262, Association for Computing Machinery (ACM).
DOI: 10.1145/838250.838251

[32] C. E. Christoffersen, 2006
Implementation of exact sensitivities in a circuit simulator using automatic differentiation.
Proceedings of ECMS 20th European Conference on Modelling and Simulation, Bonn, Germany.
DOI: 10.7148/2006-0238

[33] A. Callejo, S. H. K. Narayanan, J. García de Jalón, and B. Norris, 2014
Performance of automatic differentiation tools in the dynamic simulation of multibody systems.
Advances in Engineering Software, Volume 73, pages 35-44, Elsevier BV.
DOI: 10.1016/j.advengsoft.2014.03.002

[34] B. Minaker and F. González, 2021
Automatic differentiation in automatic generation of the linearized equations of motion.
17th International Conference on Multibody Systems, Nonlinear Dynamics, and Control (MSNDC), Online event, Volume 9, pages DETC2021-69118.
DOI: 10.1115/detc2021-69118

[35] J. García Urbieta, P. Díaz, A. J. Rodríguez, I. García, S. Armentia and F. González, 2023
Efficient Calibration of LPTN Models for Digital Twins of ePowertrain Motors.
Electric Drives Production Conference EDPC, Regensburg.

[36] United Nations, 2014
Global technical regulation 15, Worldwide harmonized Light vehicles Test Procedure.
ECE/trans/180/add.15, pages 5-24

[37] V. Madonna, P. Giangrande, and M. Galea, 2021
Influence of insulation thermal aging on the temperature assessment in electrical machines.
IEEE Transactions on Energy Conversion, Volume 36, Number 1, pages 456-467.
DOI: 10.1109/TEC.2020.3001053

[38] D. Simon, 2010
Kalman filtering with state constraints: a survey of linear and nonlinear algorithms.
IET Control Theory & Applications, Volume 4, Number 8, pages 1303-1318.
DOI: 10.1049/iet-cta.2009.0032

[39] A. Boglietti, M. Cossale, M. Popescu, and D. A. Staton, 2019
Electrical machines thermal model: Advanced calibration techniques.
IEEE Transactions on Industrial Applications, Volume 55, Number 3, pages 2620-2628.
DOI: 10.1109/TIA.2019.2897264

[40] A. Boglietti, A. Cavagnino, and D. A. Staton, 2008
Determination of critical parameters in electrical machine thermal models.
IEEE Transactions on Industrial Applications, Volume 44, Number 4, pages 1150-1159.
DOI: 10.1109/TIA.2008.926233

[41] V. Madonna, P. Giangrande, C. Gerada and M. Galea, 2019
Thermal analysis of fault-tolerant electrical machines for aerospace actuators.
IET Electric Power Applications, Volume 13, Number 7, pages 843-852.
DOI: 10.1049/iet-epa.2018.5153

[42] V. Madonna, P. Giangrande, and M. Galea, 2020
Influence of Thermal Aging on the Winding Thermal Conductivity in Low Voltage Electrical Machines.
23rd International Conference on Electrical Machines and Systems (ICEMS), Hamamatsu, Japan.
DOI: 10.23919/ICEMS50442.2020.9291167